OPEN ACCESS

GAVIN PUBLISHERS

Advances in Biochemistry and Biotechnology

Research Article

Meena D, et al. Adv Biochem Biotechnol: ABIO-179.
DOI: 10.29011/2574-7258. 000079

Biogenic Gold Nano Polymorphs with Unique Features for Enhanced Tumor Killing Efficacy and Anti-Microbial Activity

Duraisamy Meena[1], Murthy Sangeetha[2], Ramasamy Balagurunathan[2], Soudarapandian Kannan[1*]

[1]Division of Cancer Nanomedicine Laboratory, Department of Zoology, School of Life Sciences, Periyar University, Salem, Tamil Nadu, India

[2]Actinobacteria Research Laboratory, Department of Microbiology, Periyar University, Salem Tamil Nadu, India

[*]**Corresponding author:** Soudarapandian Kannan, Division of Cancer Nanomedicine Laboratory, Department of Zoology, School of Life Sciences, Periyar University, Salem - 636 011, Tamil Nadu, India. Email: skperiyaruniv@gmail.com

Citation: Meena D, Sangeetha M, Balagurunathan R, Kannan S (2019) Biogenic Gold Nano Polymorphs with Unique Features for Enhanced Tumor Killing Efficacy and Anti-Microbial Activity. Adv Biochem Biotechnol: ABIO-179. DOI: 10.29011/2574-7258. 000079

Received Date: 11 December, 2018; **Accepted Date:** 4 January, 2019; **Published Date:** 14 January, 2019

Abstract

The current study was mainly focusing on the biogenic synthesis of Gold Nanoparticles (AuNPs) using *Hibiscus sabdarffia* (leaf, stem and root) extracts and further tested against colon cancer cells and to evaluate its anti-cancer and anti-microbial activity. The biogenic AuNPs were well-known along with characterized by spectroscopic and microscopic analysis such as Ultra Violet Visible spectroscopy (UV), X-Ray Diffraction (XRD), Fourier Transformed Infrared Spectroscopy (FT-IR), Transmission Electron Microscopy (TEM), Dynamic Light Scattering (DLS) and Zeta Potential. Our finding authenticated that the AuNPs exhibited polymorphic status viz, spherical, triangular and hexagonal shapes with the typical size of 40-70nm using high, moderate and low effectiveness are seen in leaf, stem and root extract. The zeta potential bares the surface charge of AuNPs as negative. The biocompatibility of AuNPs was confirmed by incubating with RBCs and cytotoxic studies revealed a dose-dependent cytotoxic effect with half maximal inhibitory concentration value of 30±0.5µg/mL against colon cells (HT-29) at 48h incubation. In addition, AO/EtBr and DAPI staining evidenced the induction of apoptosis in cancer cells. *In vivo* toxicity assessment showed that green synthesized AuNPs have low systemic toxicity in the selected vital organs. Obviously, anti-microbial activity was conceded out for AuNPs synthesized among *H. sabdarffia*, by adopting well-diffusion method. The present study concludes that plant-based nanoparticles synthesis is easy, rapid, bio-compatible inexpensive, eco-friendly, low toxicity to non-target organs and high therapeutic efficacy in developing multifunctional AuNPs in the field of biomedicine and nanotechnology as a promising candidate for future drug delivery system.

Keywords: Anti-Cancer Activity; Anti-Microbial; Gold Nanoparticles; *Hibiscus Sabdariffa*

Introduction

Colorectal cancer is a malignant tumor arising from the inner wall of the large intestine (colon) or rectum. Colorectal cancer is the third leading cause of cancer in both men and women in the United States. Its affects over 135,000 people annually, representing 8% of all cancers. About 4.3% of people will be diagnosed with colon or rectal at some point in their lives. In modern year Nanoparticles (NPs) based drug delivery systems have shown a high degree of effectiveness in cancer managements due to their enhanced pharmacokinetics and bio distribution profiles by means of Improved Permeability and Retention (IPR) effect [1]. Metal nanoparticles are considered important, owing to their unique particle size and shape-dependent physiochemical and biological properties [2]. The noble metal nanoparticles make them an excellent resource for diversified applications, such as anti-cancer, cosmetics, coating and biocatalysts. In addition to that the metal nanoparticles are eco-benign, less toxic, and low cost effective consuming as synthesized green chemistry through methods [3]. The phytochemical of plant extract faithfully involving in reduction and stabilization reactions [4]. Further, the synthesized metal nanoparticles have chemical stability; biocompatibility, cost effectiveness and easy preparation [5,6].

Gold Nanoparticles (AuNPs) are highly stable, thermal conductive, anti-bacterial, anti-HIV and anti-malarial agents that let to be used in an extensive range of application in medicinal, chemistry [7,8]. Enthused by the easy fabrication and suitable surface functionalization, Gold Nanoparticles (AuNPs) with excellent biocompatibility have been extensively used as nanocarriers for drug and gene delivery and diagnostic agents for imaging and sensing [9-11] Gold nanoparticles are coming up as powerful agent for cancer therapy and nanosized gold particles have been evaluated against a variety of human cancer cells [5]. Gold nanoparticles are having advantages like to biocompatibility and no cytotoxicity to non-target [12]. Even though, the functionalized AuNPs have achieved hopeful therapeutic effects *in vitro* and *in vivo*, the production of resourceful drug carriers based on AuNPs with specific targeting and controllable release competence is still a dangerous challenge.

Hibiscus sabdarffia (*H. sabdarffia*) is commonly known as Indian sorrel. A recent literature survey witnessed that exhibit activities against atherosclerosis, diabetes, blood pressure suppressive, chemo protective, antioxidant, anti-tumor, anti-cancerous agents and other metabolic syndromes [13-15]. It is commonly cultivated for fiber and edible purposes and used as native medicine in India, Africa and Mexico. Interestingly, these medicinal properties are the effects of secondary metabolites present in the roselle plant. It has been also reported that, *H. sabdariffa* is a very effective anti-microbial agent and helpful in diabetes mellitus [16-19]. Previous studies have demonstrated that leaves of *H. sabdariffa* possess anticancer, hypoglycemic [20,21] antioxidant, anti-atherosclerotic [22] and estrogenic-like effects [23].

During our work, we have synthesized AuNPs via green routes using H. sabdariffa giving a special emphasize on growth of NPs at different concentration (scheme.1) shows the Optical properties of the synthesized NPs were measured using UV-visible (UV-vis) spectroscopy. Characterization of NPs had been done by X-Ray Diffraction (XRD) and Fourier Transformed Infrared Spectroscopy (FTIR). Morphology of prepared samples was analyzed by Transmission Electron Microscopy (TEM) was used to investigate the particle size. Anti-cancer and anti-microbial activity was also investigated suggesting probable mechanisms for their potential medicinal uses. Induction of AO/EtBr and DAPI are used to evidence of apoptosis. In this paper we report for the first time the biogenic synthesis of Au nanoparticles of different shapes and sizes using water soluble and plant extracts like Leaf Extract (LE), Stem Extract (SE) and Root Extract (RE) and also served as the reducing and capping agent thereby forming stable spherical, triangular, hexagonal, AuNPs. This is the first report focusing leaf, stem and root extracts of *H. sabdarffia* into cancer cells using AuNPs and also investigated the anti-cancer activity and anti-microbial activity on colon cancer cells *in vitro* and *in vivo*. Our results suggested that the biogenic AuNPs using Nano polymorphs shapes are identified by obtain effective anti-cancer activity along with plant extracts and it could be shown as a potential approach for colon cancer therapy.

Materials and Methods

Preparation of Plant Extracts

The collected plant parts of *H. sabdarffia* were washed several times with deionized water to remove impurities. Later on, the leaf, stem and root were air dried under sunlight for 1hr to eradicate the moisture completely. Then, the parts of the plant were cut into small pieces separately by 1g, 2g and 3g by adding 20mL of denionsed water using mortar and pestle. The extract was collected separate centrifuge tubes and centrifuged at 8000 rpm for 15mins. Finally, the supernatant was collected and allowed to remove any undesired impurities before further studies.

Stock Solution

Typically, 0.034 g of $HAuCl_4$ and 100mL of deionized water were mixed to get $HAuCl_4$ solution with a concentration of 1mM. Then, the total volume was transferred to a 500mL Erlenmeyer flask, refluxed for 3h and allowed to age for 24 h [24]**.**

Synthesis of Gold Nanoparticles

In brief 10ml of plant extracts were independently mixed with 30 ml of 1 mM $HAuCl_4$, allowed to keep mixing for 2hrs under stirring (150rpm) until the color of the solution changed from yellow to the ruby red color indicating the formation of AuNPs. The collections of biogenic AuNPs from aqueous solution by 8,000 rpm for 30 min, the pellet was dispersed in sterile double distilled water and poured into Petri plates and then dried in hot air oven at 40°C overnight (~12h). The dried biogenic AuNPs were scrapped out for further study.

Characterization of Synthesized AuNPs

UV-visible is a reliable technique used to determine the formation and stability of metal nanoparticles in the aqueous solution. The visual properties were observed by UV-visible spectrophotometer (UV-1800, Shimadzu) at room temperature in the range between 200-800 nm.

The FT-IR studies were done to identify the functional groups present in the *H. sabdarffia* plant extracts and their contribution in the synthesis of AuNPs. In the same way, to expect the functional group of plant extracts and their contribution in the synthesis of AuNPs were carried out on JASCO (FT-IR-400) spectrophotometer in the range of 400-4000 cm^{-1}. To determine the crystalline nature of biogenic AuNPs powder was analyzed by X-Ray Diffraction (XRD) carried out by a diffract meter (X'Pert-Phillips) with

Cu-Karadiation (45 kV/45 mA). The morphology and structure of synthesized of AuNPs was investigated by Transmission Electron Microscopy (TEM) (EM TECNAI microscope). The particle surface charge (Zeta potential) and the average size of NPs (Dynamic Light Scattering) were determined by Malvern instrument. The stability of AuNPs and synthesis of AuNPs in 10% mouse serum in DMEM at 37°C for 72 h was tested by Dynamic Light Scattering (DLS).

Cell Culture and its Maintenance

Human colon cancer cell line (HT-29) was procured from National Centre for Cell Science (Pune, India). These cell lines were maintained in DMEM media supplemented with 10% FBS, 1% L-glutamine, 1% penicillin and 1% streptomycin at 37°C in 5% CO_2 humidified incubator. Media were changed every two days, and the cells were passage by trypsinization.

In vitro Cytotoxicity Studies

3-(4, 5-Dimethylthiazol-2yl)-2, 5-diphenyltetrazolium bromide (MTT) assay was used to determine the cytotoxicity of synthesized AuNPs against (HT-29) cancerous cell and normal colon cell line (HTB-38). Briefly, cancer cells were seeded into a 96 well plate at a density of $5x10^3$ cells/well in 100µL for complete Dulbecco's Modified Eagles Medium (DMEM) containing 10% Fetal Bovine serum (FBS) and cultured for 1day at 37°C in 5% CO_2 atmosphere. Afterwards, cells were exposed to a series of AuNPs doses for further incubation of 48 h. After incubation, MTT stock solution (5mg/mL in PBS, 20µL) was added to each well and incubated for 4 h. The media were completely removed and 150µL of Dimethyl sulfoxide (DMSO) was added to each well to dissolve the formazan blue crystal and the absorbance was monitored using a microplate reader (Bio-TekELx800) at the wavelength of 490nm. For confocal microscopic analysis, HT-29 cells were seeded on cover slips placed in a 24-well plate ($1x10^5$cells/well) and grown for 48 h. Then the cells were incubated in the presence of half maximal inhibitory concentration (IC_{50}) of AuNPs at 37°C and 5% CO_2 for 48 h. OD value was subjected to start out percentage of viability by using the formula.

$$\% \text{ of cell viability} = \frac{\text{Optical density (OD) in sample well}}{\text{Optical density (OD) in control well}} \times 100$$

AO/EtBr Staining Assay

Approximately 1 µL of a dye mixture (100 mg mL^{-1} acridine Orange (AO) and 100 mg mL^{-1} Ethidium Bromide (EtBr) in distilled water) was mixed with 9 mL of cell suspension (1×10^5 cells per mL) on clean microscope cover slips. HT-29 cells were collected, washed with Phosphate Buffered Saline (PBS) (pH 7.2) and stained with 1 mL of AO/EtBr. After incubation for 2 mins, the cells were washed twice with PBS (5mins each) and visualized under a fluorescence microscope (Nikon Eclipse, Inc, Japan) at 40 x magnifications.

DAPI (4', 6-Diamidino-2-Phenylindole, Dihydrochloride) Staining

The nuclear staining of DAPI was used for visualization of nuclei of the colon cancer cells. The HT- 29 cells were treated with AuNPs for the IC_{50} concentration for 48 h at 37°C. Afterwards, 4% of formaldehyde was mixed with cells, using 0.1% triton X-100 for permeabilization of cells and then stained with 1mg/mL DAPI for 15 min in the dark. Stained images were recorded with a fluorescent microscope with the appropriate excitation filter. Percentage of apoptotic cells was determined using the following formula;

$$\% \text{ of apoptotic cells} = \frac{\text{Total number of apoptotic cells}}{\text{Total number of normal and apoptotic cells}} \times 100$$

Hemolytic Assay

Hemolytic assays were performed on the blood, expected from one healthy donor. The blood sample was newly collected by using Ethylenediamine Tetra Acetic Acid (EDTA). The blood sample 5mL was added to 8mL of Phosphate Buffered Saline (PBS: pH 7.4). The Red Blood Cells (RBCs) were isolated by centrifuge at 10,000 rpm for 5 mins and further washed three times with sterile PBS solution. Following the last wash, the RBCs were diluted to 30mL of PBS. Following to 0.2mL of diluted RBC suspension was added to AuNPs solutions at thoroughly different concentrations and mixed by vortexing. Sample tubes were kept in fixed condition at room temperature for 3 h. In conclusion, the suspension was centrifuged at 10,000 rpm for 5 mins and 100µL of supernatant of all samples was taken and its absorbance was noticed at 545nm. The percentage of hemolysis was calculated using the following formula.

$$\text{Hemolysis \%} = \frac{\text{Sample absorbance - negative control}}{\text{Positive control - negative control}} \times 100$$

Herein, RBC incubation with deionized water and PBS were used as the positive and negative controls respectively.

Assessment of Anti-Tumor Activity *in vivo*

As per the institutional Animal Ethical Committee (IAEC) of Periyar University were carried out "Accordance" with the relevant guidelines of CPCSEA with the regulatory approval PU/IAEC/085/ PO/C/07/CPCSEA/Zool/05/2016). The anti-tumor efficiency of AuNPs was assessed in tumor induced mice. Briefly, the subcutaneous dorsa of swiss albino female nude mice were inoculated with HT-29 cells ($1x10^7$) in 200µL of normal saline.

When the volume of the xeno-graft tumors reached approximately 60-85mm^3 the mice were randomly divided into 3 treatment groups and a control group (4 mice per group). For administration, treated mice were given with AuNPs at dosages of 2.0, 4.0 and 6.0mg/kg/day for 16 days through intravenous injection. In each of the AuNPs treated groups, AuNPs were injected every 3 days via caudal vein, from the first day until the 16 days (9 times). Control mice received an equal volume of PBS only. The tumor diameters were measured every 3 days' interval for each group. The tumor Volume (V) and body weight were calculated using the following formula:

$V = [\text{length} \times (\text{width})^2]/2$.

After this treatment, mice were sacrificed using a CO_2 inhalation method and the major organs such as brain, heart, liver, kidney and lung were excised and immediately fixed in 10% formalin in PBS solution. The organs were embedded in paraffin, cut into 4 µm sections using microtome, and then placed onto the glass slides. These sections were stained with Hematoxylin and Eosin (H&E) and histological images were obtained using a Nikon Eclipse 90i light microscope.

Anti-Microbial Activity of AuNPs

Six bacterial strains including both gram positive and gram negative (*Staphylococcus aureus, Staphylococcus mutans*, *Bacillus subtilis*, *Escherichia coli*, *Klebsiella pneumoniae* and *Pseudomonas aeruginosa*) were selected for the anti-bacterial activity studies. The AuNPs were tested against bacterial strains through the agar well diffusion method. Using a sterile micropipette, 100 µl of the AuNPs solution was poured onto the wells in the Luria-Bertani (LB) plates. After incubation at 37° C for 24 h, the zone of inhibition was measured. For anti-fungal activity, *Candida albicans* and *Cryptococcus neoformans* were selected. The same procedure followed as above and Sabouraud's Dextrose Agar (SDA) plates were used. Distilled water and standard antibiotics, such as erythromycin, chloramphenicol, tetracycline and vancomycin, were used as controls.

Statistical Analysis

All the measurements were made in triplicate and all values were expressed as the mean±standard error. The results were subjected to an analysis by Student's t test. The results $^*p < 0.05$ and $^{**}p < 0.01$ was considered statistically significant.

Results and Discussion

In (Figure 1a-c) UV-Visible absorption spectrum of the biogenic AuNPs, and it's confirm the complete reduction of Au ions to AuNPs in the aqueous plant extracts are using different concentration with1g, 2g and 3g. The color of the gold chloride solution vary from light yellow to ruby red is the clear evidence for the reduction of the gold ions to change NPs as aqueous spreading of AuNPs are well-known to expose deep color due to the SPR phenomenon [25-27]. In (Figure 1a) the peak range is absorbed at 544, 545, and 543 nm. The peak of the blue color is broad and clearly seen, the black and red is slightly modification. (Figure 1b) the peak range is absorbed at 545, 544, and 544 nm. The three color of the peak is broad and clearly formed. (Figure 1c) the peak range is absorbed at 544, 543 and 545 nm. (Figure 1a) From the above figure it is suggested that LE secluded later, because it contains biochemical process and more pytochemicals like, flavoniods, saponins, alkaloids and phenolic etc. So, get more time to change the formation of AuNPs [28,29] but SE and RE well isolated because it's contain less time to change the AuNPs. Most of the peak is observed by AuNPs is 543-545. In the present report, rapidly secluded SE and RE AuNPs are obtained within 2h, which could be appropriate for rapid proto-typing and scaling up the improvement of useful applications. Previously reported have obtain AuNPs by using plant extracts at a longer incubation period, such as 60 mins with Moringa oleifera petals [30] 15 mins with leaf extract of Terminalia arjuna [26] and 24 h with fruit extract of *Hovenia dulcis* [27]. Because the concentration is higher, the reaction time and bio-chemicals expected to be less in LE and RE as compared to SE because of which, the yield of NPs is very less since, its contains secondary metabolites and polyphenols. The presence of polyphenols and flavonoids in the LE leads to oxidations that result in reduction of metal cations to become neutral metal atom. The reduced metal atoms are further stabilized by the bio-ingredients present in the extract; the presence of anti-oxidant (flavonoids and polyphones) helps the gold metal to easily go through reduction process [31]. Following, the UV-Vis spectroscopic study, we carried out XRD to elucidate the crystalline structure, FT-IR study to reveal the possible structural and functional modification in the *H. sabdarffia* plant extracts followed by TEM imaging, DLS and zeta potential capacity were done, to find the size and charge present on the AuNPs.

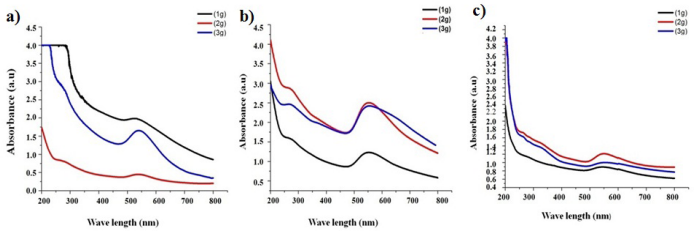

Figure 1: UV-Vis spectra of synthesized AuNPs using *Hibiscus sabdarffia* **a.** Leaf **b.** Stem and **c.** Root extract.

X-ray Diffraction Analysis of Gold Nanoparticles

The XRD pattern of the dried Au nanoparticles indicates their crystalline structure as able to seen from the diffraction pattern (Figure 2a-c). The pattern also indicates that grain size, and

preferred orientation in polycrystalline or powder solid samples. Characteristic face-centered cubic phase JCPDS No.89-3722is confirmed by the diffraction peaks corresponding to (111), (200), (220) and (311) planes respectively. In (Figure 2a) LE showed that peaks at 38.1˚, 44.2˚, 64.4˚, and 77.6˚indicating that corresponding peaks are (111) plane is more powerful than the other planes, signifying that the (111) plane is in the foremost direction and (311) have fragile when compared to other peaks. The intensity of the peaks further shows that the synthesized AuNPs are of high degree of crystalline and hence the gold chloride derivatives are able to reduce Au^{3+} and stabilize the Au nanoparticles formed [32]. (Figure 2b) SE showed that peaks at 38.5˚, 44.7˚, 65.0˚ and 77.6˚ indicating that corresponding peaks are (111) foremost position (200) planes are very closely formed (111) and the (311) planes are very fragile. (Figure 2c) root showed that peaks 38.1˚, 44.3˚, 64.6˚, and 77.4 indicating that corresponding peaks are (111) are high level and the (311) are fragile when compared to other planes of Face-Centered Cubic (FCC) respectively. The biologically synthesized AuNPs have a well-defined atomic arrangement resembling the (FCC) structure arising with bulk gold. The XRD sample thus clearly shows that the AuNPs formed by the reduction of $AuCl_4^-$ ions by H. sabdariffa plant extracts are crystalline in nature.

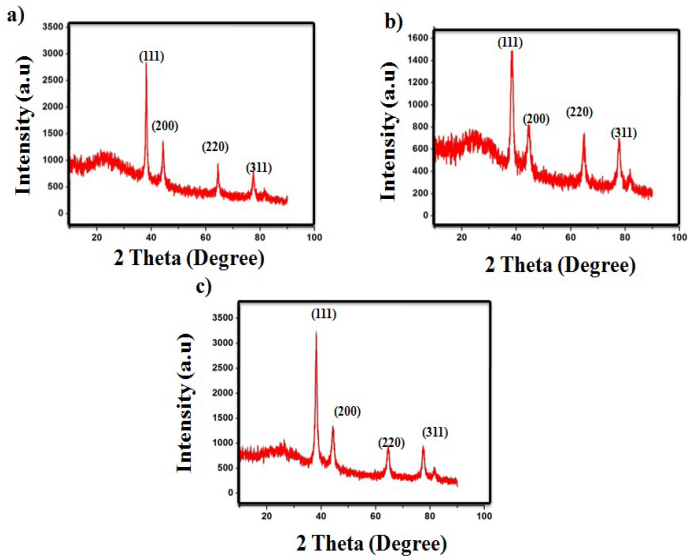

Figure 2: X-ray diffraction pattern recorded from drop coated films of the AuNPs deposited on glass substrates. The Bragg reflections are identified in the XRD pattern for: a. Leaf b. and c. Root of *H. sabdarffia.*

FT-IR characterization of AuNPs

The FT-IR spectra of the *H. sabdarffia* plant extract before and after bio-reduction have showed momentous alteration [33]. The FT-IR spectra were analyzed for detection of potential functional groups that are responsible for the excellent reduction, capping and stabilization of Au nanoparticles. In (Figure 3a and b) shows the LE of H. sabdariffa and formation of AuNPs. The bands showed that 3421-3293cm^{-1}phenols (O-H stretch), 2921-2926cm^{-1} alkanes (C-H stretch), 1632-1626cm^{-1} amine (N-H stretch), 1399-1396cm^{-1} alkanes are corresponding to asymmetrical stretching of C-H groups [34] 1230-1232cm^{-1} carboxylic acids (O-H stretch), 664-621cm^{-1} alkyl halides (C-Br stretch). In this result clearly showed that LE and AuNPs containing O-H as a functional group progress in capping the nanoparticles. Presence of LE, the bands represents different photochemical reactions like peptides/proteins, aldehydes/ketones, tartaric acid, alkaloids, and flavonoids encrusted against AuNPs during reduction process and are fundamentally thorough for stabilization of AuNPs. In (Figure 3c and d) shows the formation of AuNPs and SE of *H. sabdarffia*. The bands showed that 3347- 3193 cm^{-1} phenols (O-H stretch), 1744 -1734 cm^{-1} esters (C=O Stretch), 1625-1647 cm^{-1} amines (N-H Stretch), 1401-1431 cm^{-1} aromatics (C-C stretch), 1204-1236 cm^{-1} carboxylic acids (C-O stretch), 864-779 cm^{-1} aromatics (C-H), and 597-617 cm^{-1} alkyl halides (C-Br stretch). When compared to LE, additional groups are present in SE. There is slightly changes in stem extract and AuNPs shown the COOH group for -OH i.e. hydroxyl group the peak appeared at 1236 cm^{-1} in raw material, even though shortly than encapsulation of AuNPs (Figure 3e and f) shows the formation of AuNPs and RE of *H. sabdarffia.* The bands showed that 3326-3351 cm^{-1} phenols (O-H stretch), 2786-2925 cm^{-1} alkanes (C-H stretch), 1725-1738 cm^{-1} carboxylic acids (C=O stretch), 1507-1564 cm^{-1} (C=Cstretch), 1299 -1245 cm^{-1} alcohols (C-O stretch), 763-779 cm^{-1} alkynes (C-H stretch). In this results showed the band due to C=O stretching vibrations at 1725 cm^{-1} and the form of carboxylic group among a shift from clear RE, point out the chance that AuNPs are hurdle to proteins and anti-oxidant molecules during free amine groups and C=O, OH groups. Therefore, FT-IR study obviously shows that capping and reducing of NPs by bimolecular present in LE, SE and RE aqueous extract act of *H. sabdarffia* could be responsible for prolonged stability [35]. This indicates that gold nanoparticles synthesized using *H. sabdariffa* extracts are enclosed by some proteins and metabolites such as terpenoids have functional groups of amines, alcohols, ketones, aldehydes, and carboxylic acids [36,37].

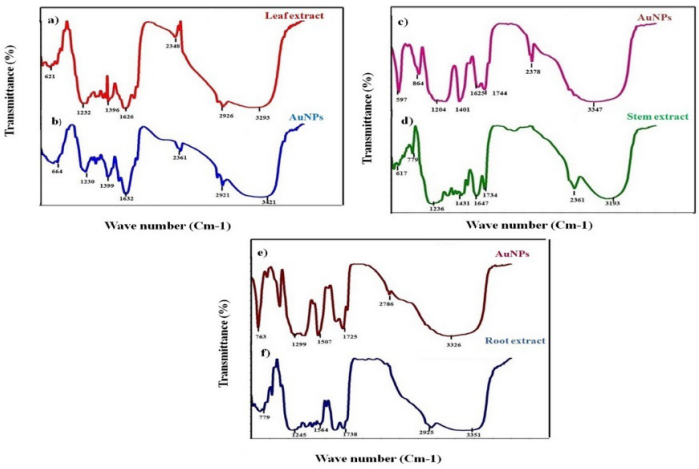

Figure 3: FT-IR spectra of synthesized AuNPs using *H. sabdarffia*. **a.** Shows leaf extract of *H. sabdarffia* **b**. Displays the gold nanoparticles were reduced from gold chloride with the LE. **c.** Illustrates the gold nanoparticles were reduced from gold chloride with the SE d. Demonstrates the stem extract of *H. sabdarffia* **e.** Explains that the gold nanoparticles were reduced by gold chloride with the RE. **f.** shows the root extract of *H. sabdarffia*.

Transmission of Electron Microscopic Analysis

TEM was used to observe the Nano polymorphs structure of synthesized biogenic AuNPs. The TEM analysis clearly reveals the formation of spherical and a small amount of hexagonal planar gold nanostructures in addition to triangular nanoparticles (Figure 4a-c). The average range TEM is 50-100nm for synthesized biogenic AuNPs. In (Figure 4a) the LE seen in spherical shape is high and triangular shape is rare, but its shows high effectiveness in LE. In (Figure 4b) the SE seen in triangular shape is high and spherical shape is rare, but its shows moderate effectiveness in SE. In (Figure 4c) the RE seen in hexagonal shape and spherical shape is rare, but its shows low effectiveness in RE. When the extract of leaf and root the secondary metabolites are present, but the stem there is no secondary metabolites are seen. In previous reported those nanoparticles synthesized using flavonoids it's indicate different morphology such as triangular, cubical, rectangular [38]. Nano triangles were formed (Figure 4a-b) owing to hasty reduction, gathering and sintering of hexagonal and sphere-shaped NPs at room temperature, reshuffle and aggregation of smaller size AuNPs [39]. The size of sphere-shaped AuNPs was between (10 to 20nm) whereas the triangular and hexagonal shaped particles were much larger (50-80nm). The irregularly shaped NPs can move easily in between the abnormally high and irregularly spread neoplastic cells compared to poly shaped or roughly spherical ones; it is reasonable to infer that these special irregular amoebic shaped is having better effect [40]. In previously showed that synthesized AuNPs, different particle size and shape using *Zingiber officinale*, An *acardium occidentale* and *Morinda citrifolia* extracts [41-45].

In present results showed that the concentration of *H. sabdarffia* responding with $HAuCl_4$ led to the expansion of spherical, triangular and hexagonal Nano polymorphs structure shows in high, moderate and low effectives in LE, SE and RE.

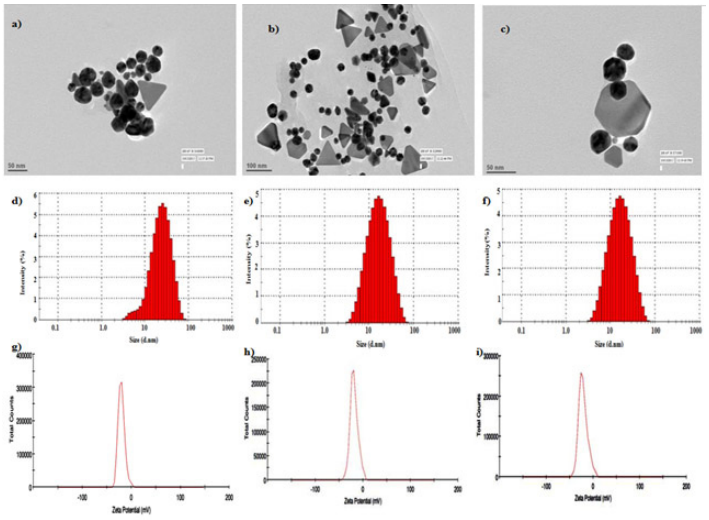

Figure 4: TEM images of synthesized gold nanoparticles and the formation of polymorphous nanoparticles which depends on the bioactive compounds present in the selected plant parts **a.** the LE of *H. sabdarffia* produces spherical shape AuNPs, whereas, the SE **(b)** forms triangle shaped gold nanoparticles. Interestingly, the RE **(c)** tailor made the gold nanoparticle as hexagonal shape. DLS used to determine the size distribution for colloid gold nanoparticles. d. shows leaf of *H. sabdarffia* **e.** shows stem of *H. sabdarffia*. **f.** shows root of *H. sabdarffia*. Zeta potential used to determine the *H. sabdarffia* extracts on AuNPs g. leaf of *H. sabdarffia* h. stem of *H. sabdarffia* i. root of *H. sabdarffi*a.

Dynamic Light Scattering

The DLS tool is recognized to determine the shell thickness of a capping or stabilizing agent persistent the metallic particles beside with the actual size of the metallic core. The size distribution and concentration graph has been shown in (Figure 4d-f). The average size of LE, SE and RE were 78nm, 92nm and 95nm respectively. The size of the AuNPs has 78nm, 92nm and 95nm, when the size of LE is low, when compared to SE and RE because of the concentration, but size of the RE was related and more poly-dispersed compared to the TEM result. The large size of particles observed by DLS is owing to the fact that the measured size also includes the bio-organic compounds persistent the foundation of the AuNPs. Therefore, a great degree of concern needs to be taken when the particle sizes are measured by various techniques for a bio-based process and need to be compared to determine their reactivity for specific applications [46].

Effect of *H.sabdariffa* Extract on AuNPs Stability

Zeta Potential (ZP) values make known information regarding the surface charge and stability of the synthesized biogenic AuNPs. In (Figure 4g-i) result showed that synthesized biogenic AuNPs obtained from negatively charged values are -20.4mV, -18.4mV and -21.3mV respectively, suggesting sophisticated stability of AuNPs. It is the significance, to mention that the AuNPs showed lower potential due to little agglomeration of the particles as indicated in TEM images while AuNPs have shown low zeta potential value because of uniform distribution of particles. However, the negative surface charge of AuNPs was observed in this deionized water, suggesting that humic substances and surfactants possibly will exists protecting Au nanoparticles with negative charge to keep them stable. The phenols groups from the *H. sabdarffia* extracts may have a stronger ability to bind metal ion, so that these compounds could form a coat over the metal nanoparticle to prevent gathering of particles. Our results agree to the recent results of Sujitha, et al. [5].

In vitro investigation of AuNPs

MTT assay was used to assess the effect of AuNPs on HT-29 cancerous cells and normal colon cell line HTB-38 cells. As shown in the (Figure 5a) AuNPs exhibited a dose-dependent cytotoxicity in HT-29 cells. However, the cytotoxicity effect of synthesized AuNPs against HTB-38 cells did not exhibit significant cytotoxicity at lower concentration and cytotoxicity increases with increasing concentration with IC_{50} values at 60±0.3µg /mL at in 48 h (Figure 5b). The IC_{50} value of biosynthesized AuNPs against HT-29 cells holds at 30±0.5µg/mL in 48 h [47]**.** It is evident from the experiment that synthesized AuNPs were able to reduce the cell viability of HT-29 cells in a dose dependent manner and can be used effectively at low concentration. This is the first study to report the cytotoxicity of synthesized AuNPs using H. sabdariffa against colon cancer cell line (HT-29). [40] reported that functionalized gold nanoparticles developed with clove bud extract inhibited 50% of the proliferation of HeLa cancer cells at 20lg/mL concentration after incubation for 48 h. Similar report of cytotoxicity at 30 µg/mL (IC_{50}) concentration was discussed for Annona squamosa leaf extract synthesized silver nanoparticles [48].

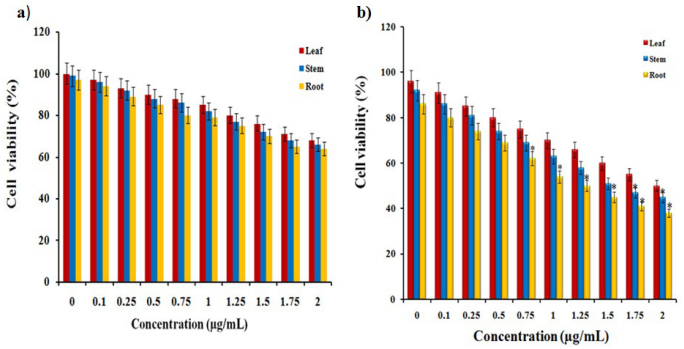

Figure 5: MTT assay results conform the in vitro cytotoxicity of AuNPs against colon cancer and normal cells for 48 h **a.** Cytotoxic effect of AuNPs on normal cell lines (HTB-39) **b.** Cytotoxic effect of AuNPs on colon cell lines (HT-29). The observed IC50 concentration was determined as 30µg/mL for the HT-29 and 60µg/mL for HTB-39 cells for 48 h.

Induction of Apoptosis by Biosynthesized AuNPs

The induction of apoptosis, after the treatment with IC_{50} concentration of AuNPs was assessed by fluorescence microscopy after staining with acridine orange/ethidium bromide (AO/EtBr). Because AO can penetrate the normal cell membrane, the cells were observed as green fluorescence, while in apoptotic cells and apoptotic bodies are formed as a result of nuclear shrinkage, blebbing and were observed as orange colored bodies whereas, necrotic cells were observed as red color fluorescence due to their loss of membrane integrity when viewed under fluorescence microscope (Figure 6). The untreated cells showed normal nuclei (smooth nuclear) whereas after treatment of HT-29 cells with AuNPs, the apoptotic nuclei (condensed or fragmented chromatin) were observed as shown in (Figure 6g). DAPI staining of the nuclei for observation of nuclear morphology helps to distinguish the apoptotic nuclei from healthy ones. Nuclear morphology analysis showed characteristic apoptotic changes, such as chromatin condensation, fragmentation of the nucleus, and formation of apoptotic bodies in the HT-29 cells. Interestingly, some studies have reported that AuNPs can also induce DNA damage and also apoptosis in cancer cells [49]. With an increase the concentration of AuNPs, number of apoptotic cells were increased, which suggested that AuNPs could induce cell apoptosis (Figure 6h).

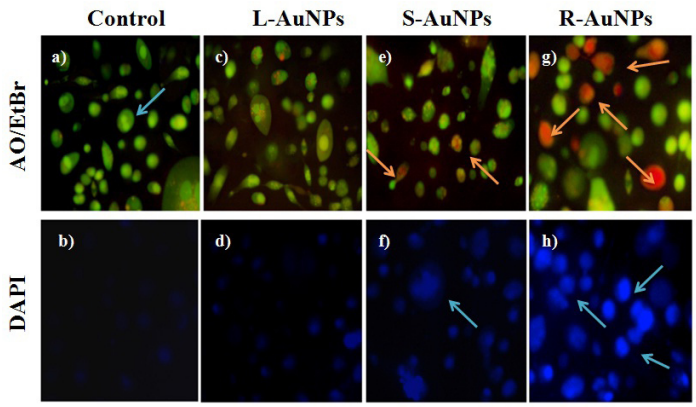

Figure 6: Bright field and fluorescence microscopy image of IC50 concentration of AuNPs treated on HT-29 cells seen in **(a-h).** Control cells are observed from bright field microscope **(a-b).** Fluorescence microscopy study of AO/EtBr stained respective control cells appear as live cells in green color and orange colored apoptotic cells whereas, the necrotic cells are appearing in red color arrows indicated by **(e-g).** The DAPI nuclear staining of control cells and AuNPs treated cells exhibited condensed form of nuclear materials in apoptotic cells which are indicated by blue color arrows **(f-h).**

Hemolysis

Hemoglobin release analysis (Table 1). In this study were used to assess the hemolytic potential of biogenic AuNPs, hemoglobin release analysis and cell morphological analysis. The RBCs were exposed to each of the NPs samples for 3 h. Hemolytic activity of control, biogenic AuNPs was resolute by measuring the release of hemoglobin. When water is added to RBCs, hemolytic takes place and the released hemoglobin is calculated. This serves as a positive control and represents absorbance to be 3.17±0.064 (100 % hemolysis). When, AuNPs were added, hemolysis was found to be <5% and is comparable to that suspended in PBS with absorbance of 0.02±0.003 (0% hemolysis) which acts as a negative control. In (Figure 7a) show the hemolytic test on the synthesized biogenic AuNPs. The supernatant from AuNPs at different concentrations is achromatic, implying that no significant hemolysis occurred. Evaluation of hemolytic properties is one of the most common tests in studies of NPs interactions with blood components [50]. Previous reported that up to 5% hemolysis is tolerable for biomaterials [51]. Thus; AuNPs at the tested concentration exhibited no significant hemolysis. The largest percentage hemolysis obtained was 1.40±0.04 % at a dosage of 30µg/mL since this is much lower than 5%, it indicates that AuNPs are hemo compatible. In present study we analysis AuNPs used to cell morphology analysis (Figure 7b) corroborated the hemoglobin release study results. The cell morphology analysis indicated that incubation of RBCs with 30µg/mL AuNPs did not result in hemolysis or change in morphology of red blood cells when compared to control sample [52].

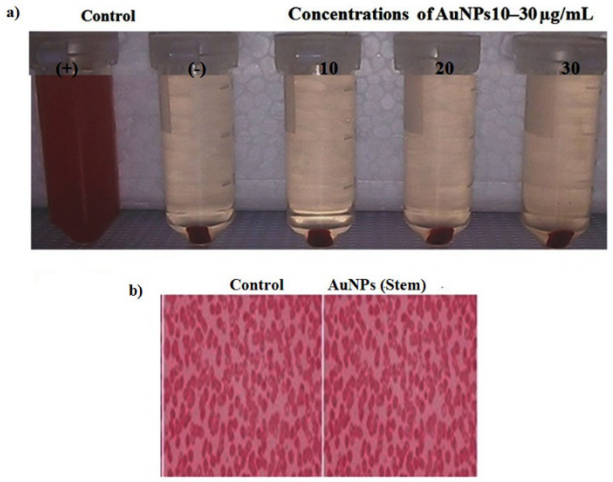

Figure 7: Hemolysis assay for synthesized AuNPs using Hibiscus sabdariffa plant extracts (leaf, stem and root) **a.** Photograph of hemolysis of RBCs incubated with concentrations 10-30µg/mL of AuNPs. The presence of red hemoglobin in the supernatant indicates the rupture of RBCs and release of hemoglobin into the buffer solution. D.I. water (-) and PBS (+) are used as positive and negative control respectively. **b.** Microscopic image (magnification of 40 x) of human RBC treated with 30 µg/mL of AuNPs. RBC without any treatment is used as control. No visible changes were observed for the gold nanoparticles. This study proves that the synthesized gold nanoparticles are hematologically safe to use as drug or drug carrier.

Au NPs (µg/mL)					
	Negative	Positive	10	20	30
Absorbance value Hemolysis (%)	3.17 ± 0.064 (100% Hemolysis)	0.02 ± 0.003 (0% hemolysis)	0.32 ± 0.012	0.59 ± 0.024	0.89 ± 0.031

Table 1. Percent Hemolysis for positive, negative control and AuNPs at different concentrations ranging from 10 to 30µg/ml for 3 h.

In vivo Anti-Tumor Activity

AuNPs considerably inhibited the proliferation of HT-29 cells in a dose dependent manner, as represent by the decrease in tumor volume and tumor weight. In addition, no separate reduction was observed in the body weight of swiss albino mice, in (Figure 8a-c) shows the LE signifying the mineral side effect of AuNPs. In (Figure 8e-f) shows that AuNPs of SE considerably inhibited the proliferation of HT-29 cells in a dose dependent manner, compared to LE slightly modified to change the tumor volume and tumor weight and also was observed in body weight (Figure 8d-e) explained the proliferation of HT-29 cells in a dose dependent manner, represent the tumor volume and tumor weight. (Figure 8f) shows no separate reduction was observed in the body weight of Swiss albino mice, signifying the mineral side effect of RE. When compared to LE and RE, the SE concentrations are clearly identified to dose dependent manner. The present investigation agrees with the recent results [47] previously, reported from our laboratory that transferring conjugated selenium nanoparticles significantly inhibited tumor growth in xenograft colon cancer mice model [53].

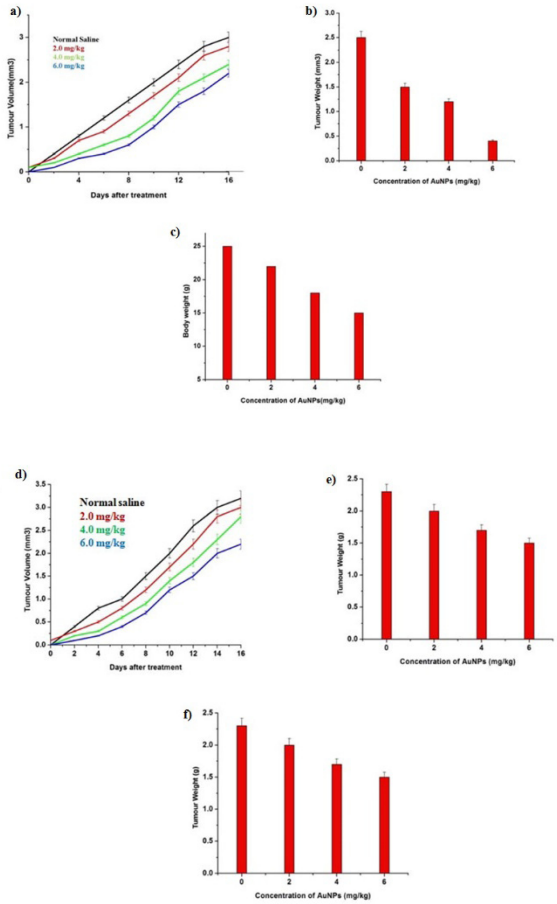

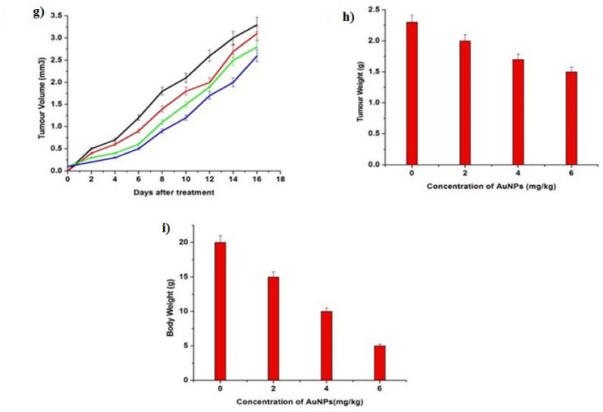

Figure 8: *In vivo* anti-cancer therapy. Tumor growth curves of four different groups of mice after treatments with different concentrations of AuNPs. The effect of tumor weight and body weight of nude mice are seen in LE, SE and RE there is no distinct reduction. Error bars are based on standard errors of the mean $^{*}p < 0.05$ and $^{**}p < 0.01$ was considered statistically significant.

Further, histological analysis of mice treated with normal saline and AuNPs exposed no important signal of damage from hematoxylin and eosin stained organ slices including lung, liver, kidney and heart (Figure 9). Histopathological studies of colon tissue included analysis of alveolar pattern. Control and treated mice did not show any injurious change in alveolar membranes and parenchyma blood vessels of lung tissue. They are slightly alteration of treated with synthesized AuNPs using *H. sabdariffa* Striated cardiac fibers and normal appearing endocardium was obvious from heart tissue from all the treatments. Other major organs such as lung, liver and kidney were also analyzed for histopathology studies [54-56].

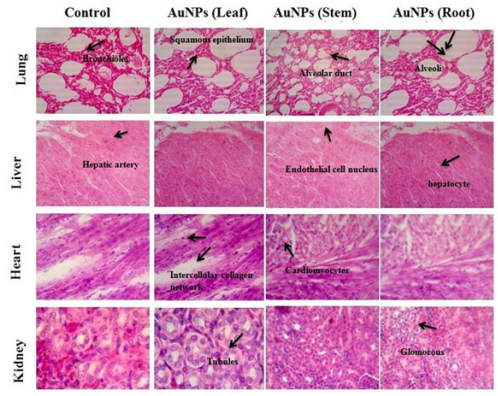

Figure 9: The histopathological analysis of major organs such as kidney, lung, liver, and heart of control and biogenic AuNPs treated mice. No significant signs of damage were noticed.

Anti-microbial Activity of AuNPs

Anti-bacterial study of AuNPs synthesized by *H. sabdariffa* plant extracts (LE, SE and RE) showed remarkable activity against all the tested bacteria and fungi. Out of three extracts root AuNPs showed more potential activity than the SE and LE extracts. In an earlier study, anti-microbial activity of plant based AuNPs are proved to be highly forceful. These results exposed that biogenic AuNPs from gum kondagogu confirmed effective anti-bacterial activity in Gram-negative than in Gram-positive bacteria [57] In (Figure 10a) AuNPs synthesized by *H. sabdarffia* RE were found to be highly effective against *K. Pneumoniae* and *E. coli* (20 and 19 mm) respectively. On the other hand, fungal activity of LE AuNPs extracts has high activity against Cryptococcus neoformans (14 mm) only. In (Figure 10b) maximum zone of inhibition (20 mm) was observed in RE AuNPs against *P. Aeruginosa* followed by *K. pneumoniae*, *E. coli*, *S. mutans* and *B. subtilis*. This result reflects the presences of synthesized AuNPs of the RE are highly effective activity than other extracts. The AuNPs may changes the permeability of the cell membrane of microbial cell by creating slits, thus inhibiting the enzyme relating activity like respiration leading to apoptosis of cells. The interaction between the AuNPs and microorganism is depending on the surface volume, size and shape of the synthesized metal nanoparticles [58, 59]

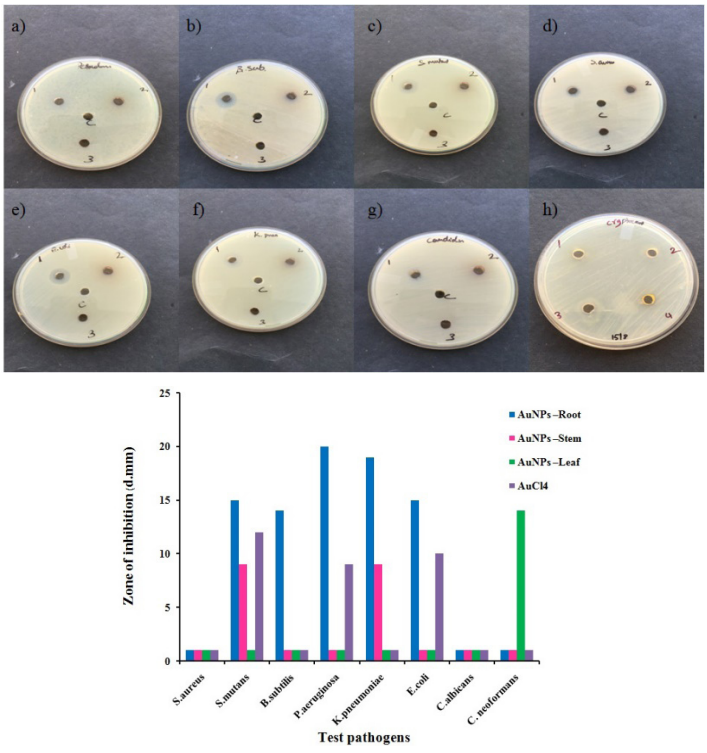

Figure 10a: Anti-bacterial and anti-fungal activity of synthesized AuNPs by *H. Sabdarffia* plant extracts **b.** zone of inhibition (mm) of *H. sabdarffia* plant extracts synthesized gold nanoparticles against various microorganisms. And graph shows that range of LE, SE and RE.

Conclusion

To the best of our knowledge, this is the first report to describe the synthesis of biogenic synthesized AuNPs showed better bio-availability, anti-cancer effect and anti- microbial against colon cancer cell line (HT-29). The synthesized biogenic AuNPs were characterized by UV, XRD, and FT-IR DLS and Zeta sizer. The TEM analysis clearly reveals the formation of spherical and a small amount of hexagonal planar gold nanostructures in addition to triangular nanoparticles. The average range TEM is 50-100 nm for synthesized biogenic AuNPs. When the extract of leaf and root the secondary metabolites are present, but the stem there is no secondary metabolites are seen. Water soluble well dispersed AuNPs is synthesized via a novel route by using the SE and RE of *H. sabdarffia*, LE contains more phytochemical present that are alkaloids, flavonoids, saponins and phenolics etc. The synthesized AuNPs exhibit good anti-bacterial and fungal activities against *E. coli*, *K. Pneumoniae* and *C. neoformans* with over 90 % inhibition. The present study reported that green synthesized method is easy, eco-friendly and bio-compatibility efficient in developing nanoparticles for assessing its therapeutic potential which could be useful in environmental and Nano medicine applications.

References

1. Shanthi K, Sreevani V, Vimala K, Kannan S (2015a) Cytotoxic effect of palladium nanoparticles synthesized from *Syzygium aromaticum* aqueous extracts and induction of apoptosis in cervical carcinoma. Springer 10: 015-06787.

2. Sathishkumar M, Sneha K, Kwak IS, Mao J, Tripathy SJ, et al. (2009) Phyto crystallization of palladium through reduction process using *Cinnamom zeylanicum* bark extract. J Hazard Mater 171: 400-404.

3. Du L, Jiang H, Liu X, Wang E (2007) Biosynthesis of gold nanoparticles assisted by *Escherichia coli* DH5α and its application on direct electrochemistry of hemoglobin. Electro chem Commun 9: 1165-1170.

4. Vivek R, Thangam R, Muthuchelian K, Gunasekaran P, Kaveri K, et al. (2012) Green biosynthesis of silver nanoparticles from *Annona squamosa* leaf extract and it's in vitro cytotoxic effect on MCF-7 cells. Process Biochem 47: 2405-2410.

5. Sujitha MV, Kannan S (2013) Green synthesis of gold nanoparticles using Citrus fruits *(Citrus limon*, *Citrus reticulata* and *Citrus sinensis*) aqueous extract and its characterization. Spectrochim. Acta A Mol. Biomol Spectrosc 102: 15-23.

6. Vimala K, Sundarraj S, Paulpandi M, Vengatesan S, Kannan S (2013) Green synthesized doxorubicin loaded zinc oxide nanoparticles regulates the Bax and Bcl-2 expression in breast and colon carcinoma. Process Biochem 49: 160-172.

7. Boruah SK, Boruah PK, Sarma P, Medhi C, Medhi OK (2012) Green Synthesis of gold nanoparticles using *Camellia Sinensis* and kinetics of the reaction. Advanced Materials Letters 3: 481-486.

8. Sharma RK, Gulati S Mehta S (2012) Preparation of Gold Nanoparticles Using Tea: A Green Chemistry Experiment. Journal of Chemical Education 89: 1316-1318.

9. Giljohann DA, Seferos DS, Daniel WL, Massich MD, Patel PC, et al. (2010) Gold Nanoparticles for Biology and Medicine. Angew Chem 49: 3280-3294.

10. Bunz UH, Rotello VM (2010) Gold Nanoparticle-Fluorophore Complexes: Sensitive and Discerning "Noses" for Biosystems Sensing. Angew Chem 49: 3268-3279.

11. Weintraub K (2013) Biomedicine: The New Gold Standard. Nature 495: S14-S16.

12. Kalita KN, Ganguli NJ (2016) *Hibiscus sabdariffa* L extract mediated green synthesis of silver nanoparticles and its use in catalytic reduction of 4-nitrophenol. Inorganic and Nano-Metal Chemistry 47: 788-793.

13. Salleh N, Runnie I, Roach D, Mohamed S, Abeywardena MY (2002) Inhibition of low-density lipoprotein oxidation and up regulation of low-density lipoprotein receptor in HepG2 cells by tropical plant extracts. J. Agric. Food Chem 50: 3693-3697.

14. Ajiboye TO, Salawu NA, Yakubu MY, Oladiji AT, Akanji MA, et al. (2011) Antioxidant and drug detoxification potentials of *Hibiscus sabdariffa* anthocyanin extract. Drug Chem. Toxicol 34: 109-115.

15. Lin HH, Chen JH, Wang CJ (2011) Chemo preventive properties and molecular mechanisms of the bioactive compounds in *Hibiscus sabdariffa* Linn. Curr Med Chem 18: 1245-1254.

16. Fullerton M, Khatiwada J, Johnson JU, Davis S (2011) Determination of Antimicrobial Activity of Sorrel (*Hibiscus sabdariffa*) on *Esherichia coli* O157:H7 Isolated from Food, Veterinary, and Clinical Samples. J. Med. Food 14: 950-956.

17. Alshami, Alharbi AE (2014) Antimicrobial activity of *Hibiscus sabdariffa* extract against uropathogenic strains isolated from recurrent urinary tract infections. Asian Pac J Trop Dis 4: 317-322.

18. Saravanan D, Lakshmi IA, Gobinath M, Kumar BG (2011) Potential Antioxidant, Hypoglycemic and Hypolipidemic Effect of Leaves of *Hibiscus platanifolius* Linn. Int J Pharm Sci Drug Res 3: 236-240.

19. Ademiluyi O, Oboh G (2012) Aqueous extracts of Roselle (*Hibiscus sabdariffa Linn*.) varieties inhibit a-amylase and a-glucosidase activities *in vitro*. J Med Food 16: 88-93.

20. Sachdewa A, Nigam R, Khemani LD (2001) Hypoglycemic effect of *Hibiscus rosa sinensis L*. leaf extract in glucose and streptozotocin induced hyperglycemic rats. Indian J Exp Biol 39: 284-286.

21. Kuriyan R, Kumar DR, Rajendran R, Kurpad AV (2010) An evaluation of the hypolipidemic effect of an extract of *Hibiscus Sabdariffa* leaves in hyperlipidemic Indians: A double blind, placebo controlled trial. BMC Complement. Altern Med 10: 27-34.

22. Chen JH, Wang CJ, Wang CP, Sheu JY, Lin CL and Lin HH (2013) *Hibiscus sabdariffa* leaf polyphenolic extract inhibits LDL oxidation and foam cell formation involving up-regulation of LXRα/ABCA1 pathway. Food Chem 141: 397-406.

23. Ali MS, Salih WM, Humida AM (1989) An estrogenic like activity of Hibiscus sabdariffa. Fitoterapia 60: 547-548.

24. Yilmaz M, Turkdemir H, AkifKilic M, Bayram E, Cicek A, et al. (2011) Biosynthesis of silver nanoparticles using leaves of *Stevia rebaudiana*. Mater Chem Phys 130: 1195-1102

25. Gopinath K, Venkatesh KS, Ilangovan R, Sankara narayanan K, Arumugam A (2013) Green synthesis of gold nanoparticles from leaf extract of *Terminalia arjuna,* for the enhanced mitotic cell division and pollen germination activity. Ind. Crops Prod 50: 737-742.

26. Basavegowda N, Idhayadhulla A, Lee YR (2014) Phyto-synthesis of gold nanoparticles using fruit extract of *Hoveniadulcis* and their biological activities. Ind Crops Prod 52: 745-751.

27. Krishnaswamy K, Orsat V (2015) Insight into the Nano dielectric properties of gold nanoparticles synthesized from maple leaf and pine needle extracts. Ind Crops Prod 66: 131-136.

28. Mishra A, Tripathy SK, Wahab R, Jeong SH, Hwang I, et al. (2011) Microbial synthesis of gold nanoparticles using the fungus *Penicillium brevicompactum* and their cytotoxic effects against mouse mayo blast cancer C2C12 cells. Appl Microbiol Biotechnol 92: 617-630.

29. Mishra A, Tripathy SK, Yun SI (2012) Fungus mediated synthesis of gold nanoparticles and their conjugation with genomic DNA isolated from *E. coli* and *S. aureus*. Process Biochem 47: 701-711.

30. Anand K, Gengan RM, Phulukdaree A, Chuturgoon A (2014) Agroforestry waste *Moringa oleifera* petals mediated green synthesis of gold nanoparticles and their anti-cancer and catalytic activity. J Ind Eng Chem 21: 1105-1111.

31. Muthukumar T, Kumari S, Sambandam B, Aravinthan A, Sastrya TP, et al. (2016) Green synthesis of gold nanoparticles and their enhanced synergistic antitumor activity using HepG2 and MCF7 cells and its antibacterial effects. Process Biochem 51: 384-391.

32. Kamal SS, Vimala J, Sahoo PK, Ghosal P, Ram S, et al. (2014) A green chemical approach for synthesis of shape anisotropic gold nanoparticles. International Nano Letters 4: 1-7.

33. Song JY, Jang HK, Kim BS (2009) Biological synthesis of gold nanoparticles using *Magnolia kobus* and *Diopyros kaki* leaf extracts. Process Biochem 44: 1133-1138.

34. Silverstein RM, Webster FX, Kiemle D (2005) Spectrometric Identification of Organic Compounds. 7th ed.

35. Jayaseelan C, Ramkumar R, Abdul Rahuman A, Perumal P (2013) Green synthesis of gold nanoparticles using seed aqueous extract of *Abelmoschus esculentus* and its antifungal activity. Ind Crops Prod 45: 423- 429.

36. Philip D (2010) Honey mediated green synthesis of silver nanoparticles. Spectrochim Acta A 78: 327-331.

37. Straumanis ME (1971) The preparation of gold nanoparticles composites using supercritical carbon dioxide. J. Monat shefte Fuer Chemie 102: 1377-1386.

38. Osonga FJ, Yazgan I, Kariuki V, Luther D, Jimenez A, et al. (2016) Greener synthesis and characterization, anti-microbial and cytotoxicity studies of gold nanoparticles of novel shapes and sizes. RSC advances: 1-14.

39. Bindhu MR, Umadevi M (2014) Silver and gold nanoparticles for sensor and antibacterial applications. Spectrochim. Acta Part A: Mol Biomol Spectrosc 128: 37-45.

40. Raghunandan D, Ravishankar B, Sharanbasava G, Mahesh DB, Harsoor V, et al. (2011) Anti-cancer studies of noble metal nanoparticles synthesized using different plant extracts**.** Cancer Nanotechnol 2: 57-65.

41. Sheny DS, Mathew J, Philip D (2012) Characterization and catalytic action of hexagonal gold nanoparticles using essential oils extracted from *Anacardium occidentale*. Spectrochim. Acta A Mol Biomol Spectrosc 97: 306-310.

42. Suman T, Rajasree SR, Ramkumar R, Rajthilak C, Perumal P (2014) The green synthesis of gold nanoparticles using an aqueous root extract of *Morinda citrifolia L*. Spectrochim. Acta Part A 118: 11-16.

43. Fazal S, Jayasree A, Sasidharan S, Koyakutty M, Nair SV, et al. (2014) Green synthesis of anisotropic gold nanoparticles for photothermal therapy of cancer. ACS Appl. Mater. Interfaces 2014.

44. Alam SN, Das S, Batuta S, Roy N, Chatterjee A, et al. (2014) *Murraya koenegii spreng*. Leaf extract: an efficient green multifunctional agent for the controlled synthesis of Au nanoparticles. ACS Sustainable Chem Eng 2: 6520-664.

45. Brayner R, Ferrari-Iliou R, Brivois N, Djediat S, Benedetti MF, et al. (2006) Toxicological impact studies based on *Escherichia coli* bacteria in ultrafine ZnO nanoparticles colloidal medium. Nano Lett 6: 866-870.

46. Kasthuri J, Veerapandian S, Rajendiran N (2009) Biological synthesis of silver and gold nanoparticles using Apiin as reducing agent. Colloids Surf B 68: 55-60.

47. Shanthi K, Vimala K, Gopi D, Kannan (2015b) Fabrication of a pH responsive DOX conjugated PEGylated palladium nanoparticle mediated drug delivery system: an *in vitro* and *in vivo* evaluation. RSC Adv 5: 44998-45014.

48. Sundarraj S, Thangam R, Sujitha MV, Vimala K, Kannan S (2014) Ligand-conjugated mesoporous silica nanorattles based on enzyme targeted prodrug delivery system for effective lung cancer therapy Toxicology and applied pharmacology 275: 232-243

49. Sanpui P, Chattopadhyay A, Ghosh SS (2011) Induction of apoptosis in cancer cells at low silver nanoparticle concentrations using chitosan nanocarrier. ACS Appl Mater Interfaces 3: 218-228.

50. Cheng FY, Su CH, Yang YS, Yeh CS, Tsai CY, et al. (2005) Characterization of aqueous dispersions of Fe(3)O(4) nanoparticles and their biomedical applications. Biomaterials 26: 729-738.

51. Singhal JP, Ray AR (2002) Synthesis of blood compatible polyamide blocks copolymers. Biomaterials 23: 1139-1145.

52. Thangam R, Sundarraj S, Vivek R, Suresh V, Sivasubramanian S, et al. (2015) Theranostic potentials of multifunctional chitosan-silver-phycoerythrin nanocomposites against triple negative breast cancer cells RSC Advances 5: 12209-12223

53. Huang Y, He L, Liu W, Fan C, Zheng W, et al. (2013) Selective cellular uptake and induction of apoptosis of cancer-targeted selenium nanoparticles. Biomaterials 34: 7106-7116.

54. Murugan C, Rayappan K, Thangam R, Bhanumathi R, Shanthi K, et al. (2016). Combinatorial nanocarrier based drug delivery approach for amalgamation of anti-tumor agents in breast cancer cells: an improved nanomedicine strategy. Nature communication, 6:34053.

55. Ponraj T, Vivek R, Paulpandi M, Rejeeth C, Nipun Babu V, et al. (2018) Mitochondrial dysfunction-induced apoptosis in breast carcinoma cells through a pH-dependent intracellular quercetin NDDS of PVPylated-TiO 2 NPs Journal of Materials Chemistry B 6: 3555-3570

56. Vivek R, NipunBabu V, Rejeeth C, Sharma A, Ponraj, et al. (2018) Multifunctional nanoparticles for tri modal photodynamic therapy-mediated photo thermal and chemotherapeutic effects Photo diagnosis and photodynamic therapy 23: 244-253

57. Reddy BG, Madhusudhan A, Ramakrishna D, Ayodhya D, Venkatesham G, et al. (2015) Green chemistry approach for the synthesis of gold nanoparticles with gum kondagogu: characterization, catalytic and antibacterial activity. J Nano struct Chem 5: 185-193.

58. Baker S, Satish S (2015) Biosynthesis of gold nanoparticles by Pseudomonas veronii AS41G inhibiting Annona squamosa L, Spectrochim. Acta Part A: Mol. Biomol. Spectrosc 15: 691-695.

59. Shanmugasundaram T, Radhakrishanan M, Gopikrishnan V, Pazhanimurugan R, Balagurunathan R (2013) A study of the bactericidal, antibiofouling, cytotoxic and antioxidant properties of action bacterially synthesized silver nanoparticles. Colloids Surf B 111: 680-687.